

Oblique parameters in gauged baryon and lepton numbers with a 125 GeV Higgs*

Yang Xiu-Yi^{1,2†}, Nie Jing^{3,1}

¹ *School of science, University of Science and*

Technology Liaoning, Anshan, Liaoning 114051, China

² *School of Physics, Shandong University, Jinan, Shandong 250100, China*

³*Department of Physics, Dalian University of Technology, Dalian 116024, China*

(Dated: November 14, 2018)

Abstract

In an extension of the standard model where baryon number and lepton number are local gauge symmetries, we analyze the effect of corrections from exotic fermions and scalars on the oblique parameters S , T , U . Because a light neutral Higgs h_0 with mass around 124 – 126 GeV strongly constrains the corresponding parameter space of this model, we also investigate the gluon fusion process $gg \rightarrow h_0$ and two photon decay of lightest neutral Higgs $h_0 \rightarrow \gamma\gamma$ at the Large Hadron Collider.

PACS numbers: 14.80.Rt, 11.10Kk, 04.50.-h

Keywords: local gauge symmetry, Baryon and Lepton numbers, Higgs

[†] yxyruxi@163.com

*Supported by National Natural Science Foundation of China (11247019) and Science and Technology Department of Liaoning (2012062)

I. INTRODUCTION

One of the main physics goals of the Large Hadron Collider (LHC) is to understand the origin of electroweak symmetry breaking, and to search for the neutral Higgs boson predicted by the standard model (SM) and its various extensions. Recently, ATLAS and CMS have reported significant excess events which are interpreted to be most probably related to a neutral Higgs with mass $m_{h_0} \sim 124 - 126$ GeV. This implies that the Higgs mechanism of breaking electroweak symmetry possibly has a solid experimental cornerstone.

The oblique parameters S , T , U [1] are extracted from electroweak precision data (EWPD) observations which probe the radiative corrections with sufficient accuracy. A light neutral Higgs with mass $124 - 126$ GeV also affects the theoretical evaluations of the oblique parameters S , T , U through loop corrections to the gauge boson propagators, which contain the neutral Higgs as a virtual field. In extensions of the SM, the corrections from exotic fields to the gauge boson propagators can be expressed in terms of shifts of the parameters S , T , U [2].

Broken baryon number (B) conservation can explain the origin of the matter-antimatter asymmetry in the Universe in a natural way. Heavy majorana neutrinos contained in the seesaw mechanism can induce the tiny observed neutrino masses [3] to explain the results of neutrino oscillation experiments. Hence, lepton number (L) is also expected to be broken. In [4], two extensions to the SM are examined, where B and L are spontaneously broken gauge symmetries around the TeV scale, while [5] also investigates the predictions for the Higgs mass and the Higgs decays in a supersymmetric model named BLMSSM, it is a minimal supersymmetric extension of the SM (MSSM) with local gauged B and L. Within the framework of the first extension of the SM with spontaneously broken B and L [4], we analyze the gluon fusion production and then decay into two photons of the Higgs with mass $m_{h_0} \sim 124 - 126$ GeV. Additionally, we also investigate the corrections from exotic fields of the oblique parameters S , T , U .

This paper is organized as follows. In Section II, we briefly summarize the main ingredients of an extension of the SM where the baryon and lepton numbers are local symmetries, then present the mass squared matrices for the neutral Higgs sector. Inspired by the new results from the ATLAS and CMS collaborations, in Section III we study in great detail the Higgs production through gluon fusion followed by the decay of the Higgs boson into two

photons. We discuss the constraints on the parameter space from the oblique parameters S , T , U in Section IV. Our conclusions are given in Section V.

II. AN EXTENSION OF THE SM WHERE BARYON AND LEPTON NUMBERS ARE LOCAL GAUGE SYMMETRIES

When baryon and lepton numbers are local gauge symmetries, one can write the gauge group as $SU(3)_C \otimes SU(2)_L \otimes U(1)_Y \otimes U(1)_B \otimes U(1)_L$. In the first extension of the SM proposed in [4], the exotic particles include new quarks Q'_L , u'_R , d'_R , new leptons l'_L , ν'_R , e'_R and three scalar singlets S_B , S_L , S along with a scalar doublet ϕ . The Yukawa couplings are written as

$$\begin{aligned}
-\mathcal{L}_Y = & \left\{ \sum_{I,J=1}^3 \left[(Y_U)_{IJ} \bar{Q}'^I_L \tilde{H} u^J_R + (Y_D)_{IJ} \bar{Q}'^I_L H d^J_R \right] + Y'_U \bar{Q}'_L Q'^c_L S_B \right. \\
& + \sum_{I=1}^3 \left[(Y_1)_I \bar{Q}'_L \tilde{\phi} u^J_R + (Y_2)_I \bar{Q}'_L \phi d^J_R \right] + h.c. \left. \right\} \\
& + \left\{ \sum_{I,J=1}^3 \left[(Y_\nu)_{IJ} \bar{L}'^I_L \tilde{H} \nu^J_R + (Y_E)_{IJ} \bar{L}'^I_L H e^J_R \right] + Y'_E \bar{L}'_L L'^c_L S_L \right. \\
& \left. + \frac{1}{2} \sum_{I,J=1}^3 (\lambda_a)_{IJ} \bar{\nu}'^{I,c}_R S^*_L \nu^J_R + \sum_{I=1}^3 (\lambda_b)_I \bar{\nu}'^{I,c}_R S_L \nu'_R + h.c. \right\}. \quad (1)
\end{aligned}$$

The scalar potential is generally given as follow:

$$\begin{aligned}
-\mathcal{L}_S = & m_H^2 H^\dagger H + m_\phi^2 \phi^\dagger \phi + m_{S_B}^2 S_B^* S_B + m_{S_L}^2 S_L^* S_L + m_S^2 S^* S \\
& + \lambda_{HH} (H^\dagger H) (H^\dagger H) + \lambda_{\phi\phi} (\phi^\dagger \phi) (\phi^\dagger \phi) + \lambda_{BB} (S_B^* S_B) (S_B^* S_B) \\
& + \lambda_{LL} (S_L^* S_L) (S_L^* S_L) + \lambda_{SS} (S^* S) (S^* S) + \lambda_{H\phi} (H^\dagger H) (\phi^\dagger \phi) \\
& + \lambda_{HB} (H^\dagger H) (S_B^* S_B) + \lambda_{HL} (H^\dagger H) (S_L^* S_L) + \lambda_{HS} (H^\dagger H) (S^* S) \\
& + \lambda_{\phi B} (\phi^\dagger \phi) (S_B^* S_B) + \lambda_{\phi L} (\phi^\dagger \phi) (S_L^* S_L) + \lambda_{\phi S} (\phi^\dagger \phi) (S^* S) \\
& + \lambda_{BL} (S_B^* S_B) (S_L^* S_L) + \lambda_{BS} (S_B^* S_B) (S^* S) + \lambda_{LS} (S_L^* S_L) (S^* S) \\
& + \lambda'_{H\phi} (H^\dagger \phi) (\phi^\dagger H) + [\mu_1 (H^\dagger \phi) S + \mu_2 S_B^* S^2 + h.c.]. \quad (2)
\end{aligned}$$

When the $SU(2)_L$ doublet H and $SU(2)_L$ singlets S_B , S_L acquire the nonzero vacuum expectation values (VEVs) v , $v_{B,L}$,

$$H = \begin{pmatrix} G^+ \\ \frac{1}{\sqrt{2}}(v + H_0 + iG^0) \end{pmatrix},$$

$$\begin{aligned}
S_B &= \frac{1}{\sqrt{2}}(v_B + S_B^0 + iG_B^0), \\
S_L &= \frac{1}{\sqrt{2}}(v_L + S_L^0 + iG_L^0),
\end{aligned} \tag{3}$$

the local gauge symmetry $SU(2)_L \otimes U(1)_Y \otimes U(1)_B \otimes U(1)_L$ is broken down to the electromagnetic symmetry $U(1)_e$, where G^+ , G^0 , G_B^0 and G_L^0 denote the massless Goldstone bosons. Correspondingly, the mass terms for the neutral Higgs are formulated as

$$-\mathcal{L}_{mass}^H = \frac{1}{2} \begin{pmatrix} H_0, & S_B^0, & S_L^0 \end{pmatrix} m_{CPE}^2 \begin{pmatrix} H_0 \\ S_B^0 \\ S_L^0 \end{pmatrix}, \tag{4}$$

where the symmetric 3×3 mass squared matrix m_{CPE}^2 is

$$m_{CPE}^2 = \begin{pmatrix} 2\lambda_{HH}v^2 & \lambda_{HB}vv_B & \lambda_{HL}vv_L \\ \lambda_{HB}vv_B & 2\lambda_{BB}v_B^2 & \lambda_{BL}v_Bv_L \\ \lambda_{HL}vv_L & \lambda_{BL}v_Bv_L & 2\lambda_{LL}v_L^2 \end{pmatrix}. \tag{5}$$

Through the orthogonal 3×3 transformation matrix Z_{CPE} , the mass squared matrix m_{CPE}^2 can be diagonalized as

$$Z_{CPE}^T m_{CPE}^2 Z_{CPE} = \begin{pmatrix} m_{H_1^0}^2, & m_{H_2^0}^2, & m_{H_3^0}^2 \end{pmatrix}, \tag{6}$$

where $m_{H_1^0} = m_{h_0} \simeq 125$ GeV.

In a similar way, we can write the $SU(2)_L$ doublet ϕ and the $SU(2)_L$ singlet S as

$$\begin{aligned}
\phi &= \begin{pmatrix} \phi^+ \\ \frac{1}{\sqrt{2}}(\phi_R^0 + i\phi_I^0) \end{pmatrix}, \\
S &= \frac{1}{\sqrt{2}}(S_R^0 + iS_I^0).
\end{aligned} \tag{7}$$

As the local gauge symmetry $SU(2)_L \otimes U(1)_Y \otimes U(1)_B \otimes U(1)_L$ is broken down to the electromagnetic symmetry $U(1)_e$, the terms in square brackets in Eq. (2) induce mixing among the neutral scalar particles ϕ_R^0 , ϕ_I^0 , S_R^0 , S_I^0 , and the mass terms are written as

$$-\mathcal{L}_{mass}^\Phi = \frac{1}{2} \begin{pmatrix} \phi_R^0, & S_R^0, & \phi_I^0, & S_I^0 \end{pmatrix} m_{CPM}^2 \begin{pmatrix} \phi_R^0 \\ S_R^0 \\ \phi_I^0 \\ S_I^0 \end{pmatrix}, \tag{8}$$

with the symmetric 4×4 mass squared matrix m_{CPM}^2 being

$$m_{CPM}^2 = \begin{pmatrix} m_\phi^2 & \sqrt{2}v\Re(\mu_1) & 0 & -\sqrt{2}v\Im(\mu_1) \\ \sqrt{2}v\Re(\mu_1) & m_s^2 + 2\sqrt{2}v_B\Re(\mu_2) & 0 & -2\sqrt{2}v_B\Im(\mu_2) \\ 0 & 0 & m_\phi^2 & -\sqrt{2}v\Re(\mu_1) \\ -\sqrt{2}v\Im(\mu_1) & -2\sqrt{2}v_B\Im(\mu_2) & -\sqrt{2}v\Re(\mu_1) & m_s^2 + 2\sqrt{2}v_B\Re(\mu_2) \end{pmatrix}. \quad (9)$$

We also diagonalize the mass squared matrix m_{CPM}^2 through the 4×4 orthogonal rotation Z_{CPM} :

$$Z_{CPM}^T m_{CPM}^2 Z_{CPM} = \left(m_{\Phi_1}^2, m_{\Phi_2}^2, m_{\Phi_3}^2, m_{\Phi_4}^2 \right). \quad (10)$$

Similarly, the mass for the charged scalar ϕ^\pm is expressed by

$$m_{\phi^\pm}^2 = \frac{1}{2}m_\phi^2 - \frac{1}{2}\lambda'_{H\phi} v^2. \quad (11)$$

Since the field ϕ does not get a nonzero VEV after the electroweak symmetry is broken down, there is no mass mixing between the exotic quarks and the SM quarks.

In the left-handed basis $(\nu_L^I, \nu_L^I, \nu_R^I, \nu_R^I)$, ($I = 1, 2, 3$), the mass matrix for neutrinos is given by the 8×8 matrix

$$\mathcal{M}_n = \begin{pmatrix} 0_{3 \times 3} & (M_D)_{3 \times 5} \\ (M_D^T)_{5 \times 3} & (M_N)_{5 \times 5} \end{pmatrix}. \quad (12)$$

Here, the 3×5 matrix M_D is written as

$$M_D = \left(0_{3 \times 2}, \frac{v}{\sqrt{2}}(Y_\nu^*)_{3 \times 3} \right), \quad (13)$$

and the 5×5 matrix M_N is

$$M_N = \begin{pmatrix} 0, & \frac{v}{\sqrt{2}}Y_\nu'^*, & 0_{1 \times 3} \\ \frac{v}{\sqrt{2}}Y_\nu'^*, & 0, & \frac{v}{\sqrt{2}}(\lambda_b^*)_{1 \times 3} \\ 0_{3 \times 1}, & \frac{v}{\sqrt{2}}(\lambda_b^\dagger)_{3 \times 1}, & \frac{v}{\sqrt{2}}(\lambda_a^\dagger)_{3 \times 3} \end{pmatrix}, \quad (14)$$

Integrating the heavy freedoms out, we get the following mass matrix for three light neutrinos:

$$\mathcal{M}_\nu = -M_D M_N^{-1} M_D^T, \quad (15)$$

which is diagonalized by the Pontecorvo-Maki-Nakagawa-Sakata matrix U_{PMNS}

$$U_{PMNS}^T \mathcal{M}_\nu U_{PMNS} = \text{diag}(m_{\nu_1}, m_{\nu_2}, m_{\nu_3}). \quad (16)$$

Meanwhile, the Majorana mass matrix M_N is similarly diagonalized by a 5×5 matrix Z_N

$$Z_N^T M_N Z_N = \text{diag}(m_{N_1}, m_{N_2}, m_{N_3}, m_{N_4}, m_{N_5}). \quad (17)$$

III. THE $gg \rightarrow h_0 \rightarrow \gamma\gamma$ PROCESS IN GAUGED BARYON AND LEPTON NUMBERS

At the LHC, the Higgs is produced chiefly through gluon fusion. In the SM, the leading order (LO) contributions originate from the one-loop diagram, which involves virtual top quarks. The cross section for this process is known to the next-to-next-to-leading order (NNLO) [6], which can enhance the LO result by 80-100%. Furthermore, any new particle which couples strongly with the Higgs can significantly modify this cross section. In the extension of the SM considered here, the LO decay width for the process $h_0 \rightarrow gg$ is given by (see [7] and references therein)

$$\Gamma_{NP}(h_0 \rightarrow gg) = \frac{G_F \alpha_s^2 m_{h_0}^3 |(Z_{CPE})_{11}|^2}{64\sqrt{2}\pi^3} \left| A_{1/2}(x_t) + A_{1/2}(x_{t'}) + A_{1/2}(x_{b'}) \right|^2, \quad (18)$$

where $x_a = m_a^2/(4m_{h_0}^2)$, $a = t, t', b'$, and the loop function $A_{1/2}$ is defined in the Appendix.

The Higgs to diphoton decay is also obtained from loop diagrams. The LO contributions are derived from the one-loop diagrams containing virtual charged gauge bosons W^\pm or virtual top quarks in the SM. In this model, the additional charged scalar ϕ^\pm and exotic fermions t', b', τ' contribute corrections to the decay width of the Higgs to diphoton at LO. The corresponding expression is written as

$$\begin{aligned} \Gamma_{NP}(h_0 \rightarrow \gamma\gamma) = & \frac{G_F \alpha^2 m_{h_0}^3}{128\sqrt{2}\pi^3} \left| (Z_{CPE})_{11} \left(\frac{4}{3} A_{1/2}(x_t) + \frac{4}{3} A_{1/2}(x_{t'}) + \frac{1}{3} A_{1/2}(x_{b'}) \right) \right. \\ & + A_{1/2}(x_{\tau'}) + A_1(x_W) \left. \right) + \frac{8m_W^2 s_W^2}{e^2 m_{\phi^\pm}^2} \left(\lambda_{H\phi} (Z_{CPE})_{11} + \frac{v_B}{v} \lambda_{\phi B} (Z_{CPE})_{21} \right. \\ & \left. + \frac{v_L}{v} \lambda_{\phi L} (Z_{CPE})_{31} \right) A_0(x_{\phi^\pm}) \left. \right|^2, \quad (19) \end{aligned}$$

where the concrete expressions for the loop functions A_0, A_1 are given in the Appendix.

The Higgs discovery from both the ATLAS and CMS experiments have observed an excess in Higgs production and decay into the diphoton channel which is a factor $1.4 \sim 2$ times

larger than the SM expectations. The observed signal for the diphoton channels is quantified by the ratio

$$R_{\gamma\gamma} = \frac{\Gamma_{NP}(h_0 \rightarrow gg)\Gamma_{NP}(h_0 \rightarrow \gamma\gamma)}{\Gamma_{SM}(h_0 \rightarrow gg)\Gamma_{SM}(h_0 \rightarrow \gamma\gamma)}, \quad (20)$$

where we assume that all exotic fields are heavier than the lightest Higgs h_0 . The current value of this ratio is as follows [8, 9]:

$$\begin{aligned} \text{ATLAS : } R_{\gamma\gamma} &= 1.90 \pm 0.5, \\ \text{CMS : } R_{\gamma\gamma} &= 1.56 \pm 0.43, \\ \text{ATLAS + CMS : } R_{\gamma\gamma} &= 1.71 \pm 0.33. \end{aligned} \quad (21)$$

Note that the combination of the ATLAS and CMS results is taken from [10].

IV. CORRECTIONS TO THE OBLIQUE PARAMETERS

A common approach to constrain physics beyond the SM is to use global electroweak fitting through the oblique parameters S , T , U [1]. In the SM, electroweak precision tests imply a relationship between m_{h_0} and m_z . In the model considered here, the electroweak precision tests also strongly constrain the mass spectrum and relevant couplings.

Here, we adopt the definitions of the oblique parameters S , T , U given in [1, 11]:

$$\begin{aligned} S &= 16\pi \left\{ \frac{\Pi_{33}(m_z^2) - \Pi_{33}(0)}{m_z^2} - \frac{\Pi_{3Q}(m_z^2) - \Pi_{3Q}(0)}{m_z^2} \right\}, \\ T &= 4\pi \frac{\Pi_{11}(0) - \Pi_{33}(0)}{m_z^2 s_w^2 c_w^2}, \\ U &= 16\pi \left\{ \frac{\Pi_{11}(m_z^2) - \Pi_{11}(0)}{m_z^2} - \frac{\Pi_{33}(m_z^2) - \Pi_{33}(0)}{m_z^2} \right\}, \end{aligned} \quad (22)$$

where $s_w = \sin \theta_w$ and $c_w = \cos \theta_w$ with the Weinberg angle θ_w defined at the energy scale $\mu = m_z$. In the above definitions, Π_{11} and Π_{33} are the vacuum polarizations of isospin currents, and Π_{3Q} is the vacuum polarization of one isospin and one hypercharge current.

By comparing the measurable electroweak observables with the theoretical predictions, one finds the fitted values[12]

$$\begin{aligned} \Delta S &= S - S_{\text{SM}} = 0.04 \pm 0.10, \\ \Delta T &= T - T_{\text{SM}} = 0.05 \pm 0.11, \\ \Delta U &= U - U_{\text{SM}} = 0.08 \pm 0.11. \end{aligned} \quad (23)$$

As mentioned above, there is no mass mixing between the exotic quarks and the SM quarks. The corresponding corrections to the oblique parameters from exotic quarks are

$$\begin{aligned}
\Delta S_{Q'} &= \frac{1}{\pi} \left\{ \int_0^1 dx x(1-x) \ln \frac{m_{b'}^2 - x(1-x)m_z^2}{m_{t'}^2 - x(1-x)m_z^2} - \frac{3m_{t'}^2}{2m_z^2} \int_0^1 dx \ln \frac{m_{t'}^2 - x(1-x)m_z^2}{m_{t'}^2} \right. \\
&\quad \left. - \frac{3m_{b'}^2}{2m_z^2} \int_0^1 dx \ln \frac{m_{b'}^2 - x(1-x)m_z^2}{m_{b'}^2} \right\}, \\
\Delta T_{Q'} &= -\frac{3}{4\pi s_w^2 c_w^2} \left\{ \frac{m_{t'}^2}{m_z^2} \int_0^1 dx x \ln \frac{xm_{t'}^2 + (1-x)m_{b'}^2}{m_{t'}^2} + \frac{m_{b'}^2}{m_z^2} \int_0^1 dx (1-x) \ln \frac{xm_{t'}^2 + (1-x)m_{b'}^2}{m_{b'}^2} \right\}, \\
\Delta U_{Q'} &= \frac{1}{\pi} \left\{ 3 \int_0^1 dx x(1-x) \ln \frac{[xm_{t'}^2 + (1-x)m_{b'}^2 - x(1-x)m_z^2]^2}{[m_{t'}^2 - x(1-x)m_z^2][m_{b'}^2 - x(1-x)m_z^2]} \right. \\
&\quad - 3 \int_0^1 dx \left(x \frac{m_{t'}^2}{m_z^2} + (1-x) \frac{m_{b'}^2}{m_z^2} \right) \ln \frac{xm_{t'}^2 + (1-x)m_{b'}^2 - x(1-x)m_z^2}{xm_{t'}^2 + (1-x)m_{b'}^2} \\
&\quad \left. - \frac{3m_{t'}^2}{2m_z^2} \int_0^1 dx \ln \frac{m_{t'}^2 - x(1-x)m_z^2}{m_{t'}^2} - \frac{3m_{b'}^2}{2m_z^2} \int_0^1 dx \ln \frac{m_{b'}^2 - x(1-x)m_z^2}{m_{b'}^2} \right\}. \tag{24}
\end{aligned}$$

Here, $m_{b'}$ and $m_{t'}$ denote the masses of the charged $-1/3$ exotic quark b' and the charged $2/3$ exotic quark t' , respectively.

In a similar way, there is no mass mixing between the exotic charged leptons and the SM leptons. Ignoring the tiny mixing between the left-handed neutrinos and heavy majorana neutrinos, we write the corrections to the oblique parameters from exotic leptons as

$$\begin{aligned}
\Delta S_{L'} &= \frac{1}{\pi} \sum_{i,j=1}^5 (Z_N)_{1i} (Z_N^\dagger)_{i1} (Z_N)_{1j} (Z_N^\dagger)_{j1} \left\{ -\frac{1}{2} \int_0^1 dx \left(x \frac{m_{N_i}^2}{m_z^2} + (1-x) \frac{m_{N_j}^2}{m_z^2} \right) \right. \\
&\quad \times \ln \frac{xm_{N_i}^2 + (1-x)m_{N_j}^2 - x(1-x)m_z^2}{xm_{N_i}^2 + (1-x)m_{N_j}^2} - \frac{m_{\tau'}^2}{2m_z^2} \int_0^1 dx \ln \frac{m_{\tau'}^2 - x(1-x)m_z^2}{m_{\tau'}^2} \\
&\quad \left. + \int_0^1 dx x(1-x) \ln \frac{xm_{N_i}^2 + (1-x)m_{N_j}^2 - x(1-x)m_z^2}{m_{\tau'}^2 - x(1-x)m_z^2} \right\}, \\
\Delta T_{L'} &= -\frac{1}{4\pi s_w^2 c_w^2} \sum_{i,j=1}^5 (Z_N)_{1i} (Z_N^\dagger)_{i1} (Z_N)_{1j} (Z_N^\dagger)_{j1} \left\{ \frac{m_{N_i}^2}{m_z^2} \int_0^1 dx \ln \frac{xm_{N_i}^2 + (1-x)m_{\tau'}^2}{xm_{N_i}^2 + (1-x)m_{N_j}^2} \right. \\
&\quad \left. + \frac{m_{\tau'}^2}{m_z^2} \int_0^1 dx (1-x) \ln \frac{xm_{N_i}^2 + (1-x)m_{\tau'}^2}{m_{\tau'}^2} \right\}, \\
\Delta U_{L'} &= \frac{1}{\pi} \sum_{i,j=1}^5 (Z_N)_{1i} (Z_N^\dagger)_{i1} (Z_N)_{1j} (Z_N^\dagger)_{j1} \left\{ \frac{m_{\tau'}^2}{2m_z^2} \int_0^1 dx \ln \frac{m_{\tau'}^2 - x(1-x)m_z^2}{m_{\tau'}^2} \right. \\
&\quad + \int_0^1 dx x(1-x) \ln \frac{[xm_{N_i}^2 + (1-x)m_{\tau'}^2 - x(1-x)m_z^2]^2}{(xm_{N_i}^2 + (1-x)m_{N_j}^2 - x(1-x)m_z^2)(m_{\tau'}^2 - x(1-x)m_z^2)} \\
&\quad \left. - \int_0^1 dx \left(x \frac{m_{N_i}^2}{m_z^2} + (1-x) \frac{m_{\tau'}^2}{m_z^2} \right) \ln \frac{xm_{N_i}^2 + (1-x)m_{\tau'}^2 - x(1-x)m_z^2}{xm_{N_i}^2 + (1-x)m_{\tau'}^2} \right\}
\end{aligned}$$

$$+\frac{1}{2} \int_0^1 dx \left(x \frac{m_{N_i}^2}{m_Z^2} + (1-x) \frac{m_{N_j}^2}{m_Z^2} \right) \ln \frac{xm_{N_i}^2 + (1-x)m_{N_j}^2 - x(1-x)m_Z^2}{xm_{N_i}^2 + (1-x)m_{N_j}^2} \}. \quad (25)$$

Here, the 5×5 unitary matrix Z_N is the mixing matrix for heavy majorana neutrinos, m_{N_i} ($i = 1, 2, \dots, 5$) are the corresponding masses of the heavy neutrinos, and $m_{\tau'}$ is the mass of the charged exotic lepton τ' .

As the radiative corrections to the self energy of gauge bosons originate from three CP-even Higgs (h_0, H_2^0, H_3^0), the corresponding contributions to the oblique parameters are given by

$$\begin{aligned} \Delta S_H &= \frac{1}{\pi} \sum_{i=1}^3 (Z_{CPE})_{1i}^2 \left\{ \frac{1}{2} \int_0^1 dx x(1-x) \ln \frac{x^2 m_Z^2 + (1-x)m_{H_i^0}^2}{m_Z^2} \right. \\ &\quad \left. + \int_0^1 dx \left(1 - \frac{x}{2} - (1-x) \frac{m_{H_i^0}^2}{2m_Z^2} \right) \ln \frac{x^2 m_Z^2 + (1-x)m_{H_i^0}^2}{xm_Z^2 + (1-x)m_{H_i^0}^2} \right\}, \\ \Delta T_H &= \frac{1}{4\pi s_W^2 c_W^2} \sum_{i=1}^3 (Z_{CPE})_{1i}^2 \left\{ - \int_0^1 dx \left(1 - \frac{x}{2} - (1-x) \frac{m_{H_i^0}^2}{2m_Z^2} \right) \right. \\ &\quad \times \ln \frac{xm_Z^2 + (1-x)m_{H_i^0}^2}{m_Z^2} \\ &\quad \left. + \int_0^1 dx \left(\left(1 - \frac{x}{2} \right) c_W^2 - (1-x) \frac{m_{H_i^0}^2}{2m_Z^2} \right) \ln \frac{xm_W^2 + (1-x)m_{H_i^0}^2}{m_Z^2} \right\}, \\ \Delta U_H &= \frac{1}{\pi} \sum_{i=1}^3 (Z_{CPE})_{1i}^2 \left\{ \frac{1}{2} \int_0^1 dx \left(x^2 + (1-x) \frac{m_{H_i^0}^2}{m_Z^2} \right) \right. \\ &\quad \times \ln \frac{x^2 m_Z^2 + (1-x)m_{H_i^0}^2}{m_Z^2} - \int_0^1 dx \ln \frac{x^2 m_Z^2 + (1-x)m_{H_i^0}^2}{xm_Z^2 + (1-x)m_{H_i^0}^2} \\ &\quad - \frac{1}{2} \int_0^1 dx \left(x + (1-x) \frac{m_{H_i^0}^2}{m_Z^2} \right) \ln \frac{xm_Z^2 + (1-x)m_{H_i^0}^2}{m_Z^2} \\ &\quad \left. + \int_0^1 dx \left(\left(1 - \frac{x}{2} \right) c_W^2 - (1-x) \frac{m_{H_i^0}^2}{2m_Z^2} \right) \ln \frac{xm_W^2 + (1-x)m_{H_i^0}^2 - x(1-x)m_Z^2}{xm_W^2 + (1-x)m_{H_i^0}^2} \right. \\ &\quad \left. + \frac{1}{2} \int_0^1 dx x(1-x) \ln \frac{xm_W^2 + (1-x)m_{H_i^0}^2 - x(1-x)m_Z^2}{m_Z^2} \right\}. \quad (26) \end{aligned}$$

Here we adopt the notation H_1^0 to represent the lightest neutral Higgs h_0 . In addition, the contributions from Φ_i^0 and ϕ^\pm to the oblique parameters are formulated as follows

$$\Delta S_\phi = \frac{1}{2\pi} \left\{ \sum_{i,j}^4 (Z_{CPM})_{1i}^2 (Z_{CPM})_{3j}^2 \left[- \int_0^1 dx \left(x \frac{m_{\Phi_i^0}^2}{m_Z^2} + (1-x) \frac{m_{\Phi_j^0}^2}{m_Z^2} \right) \right. \right.$$

$$\begin{aligned}
& \times \ln \frac{xm_{\Phi_i^0}^2 + (1-x)m_{\Phi_j^0}^2 - x(1-x)m_Z^2}{xm_{\Phi_i^0}^2 + (1-x)m_{\Phi_j^0}^2} \\
& - \int_0^1 dx x(1-x) \ln \frac{xm_{\Phi_i^0}^2 + (1-x)m_{\Phi_j^0}^2 - x(1-x)m_Z^2}{m_{\phi^\pm}^2 - x(1-x)m_Z^2} \Big] \\
& + \frac{m_{\phi^\pm}^2}{m_Z^2} \int_0^1 dx \ln \frac{m_{\phi^\pm}^2 - x(1-x)m_Z^2}{m_{\phi^\pm}^2} \Big\} , \\
\Delta T_\phi = & \frac{1}{8\pi s_W^2 c_W^2} \left\{ - \sum_{i=1}^4 [(Z_{CPM})_{1i}^2 + (Z_{CPM})_{3i}^2] \right. \\
& \times \left[\frac{m_{\phi^\pm}^2}{m_Z^2} \int_0^1 dx x \ln \frac{xm_{\phi^\pm}^2 + (1-x)m_{\Phi_i^0}^2}{m_{\phi^\pm}^2} + \frac{m_{\Phi_i^0}^2}{m_Z^2} \int_0^1 dx x \ln \frac{xm_{\Phi_i^0}^2 + (1-x)m_{\phi^\pm}^2}{m_{\Phi_i^0}^2} \right] \\
& + \sum_{i,j}^4 (Z_{CPM})_{1i}^2 (Z_{CPM})_{3j}^2 \int_0^1 dx \left(x \frac{m_{\Phi_i^0}^2}{m_Z^2} + (1-x) \frac{m_{\Phi_j^0}^2}{m_Z^2} \right) \\
& \times \ln \frac{xm_{\Phi_i^0}^2 + (1-x)m_{\Phi_j^0}^2}{m_{\Phi_i^0}^2} \Big\} , \\
\Delta U_\phi = & \frac{1}{2\pi} \left\{ - \sum_{i=1}^4 [(Z_{CPM})_{1i}^2 + (Z_{CPM})_{3i}^2] \left[\int_0^1 dx \left(x \frac{m_{\phi^\pm}^2}{m_Z^2} + (1-x) \frac{m_{\Phi_i^0}^2}{m_Z^2} \right) \right. \right. \\
& \times \ln \frac{xm_{\phi^\pm}^2 + (1-x)m_{\Phi_i^0}^2 - x(1-x)m_Z^2}{xm_{\phi^\pm}^2 + (1-x)m_{\Phi_i^0}^2} \\
& + \frac{1}{2} \int_0^1 dx x(1-x) \ln \frac{xm_{\phi^\pm}^2 + (1-x)m_{\Phi_i^0}^2 - x(1-x)m_Z^2}{m_{\phi^\pm}^2 - x(1-x)m_Z^2} \Big] \\
& + \sum_{i,j}^4 (Z_{CPM})_{1i}^2 (Z_{CPM})_{3j}^2 \left[\int_0^1 dx \left(x \frac{m_{\Phi_i^0}^2}{m_Z^2} + (1-x) \frac{m_{\Phi_j^0}^2}{m_Z^2} \right) \right. \\
& \times \ln \frac{xm_{\Phi_i^0}^2 + (1-x)m_{\Phi_j^0}^2 - x(1-x)m_Z^2}{xm_{\Phi_i^0}^2 + (1-x)m_{\Phi_j^0}^2} \\
& + \int_0^1 dx x(1-x) \ln \frac{xm_{\Phi_i^0}^2 + (1-x)m_{\Phi_j^0}^2 - x(1-x)m_Z^2}{xm_{\Phi_i^0}^2 + (1-x)m_{\phi^\pm}^2 - x(1-x)m_Z^2} \\
& + \int_0^1 dx x(1-x) \ln \frac{xm_{\Phi_i^0}^2 + (1-x)m_{\Phi_j^0}^2 - x(1-x)m_Z^2}{xm_{\phi^\pm}^2 + (1-x)m_{\Phi_j^0}^2 - x(1-x)m_Z^2} \Big] \\
& \left. + \frac{m_{\phi^\pm}^2}{m_Z^2} \int_0^1 dx \ln \frac{m_{\phi^\pm}^2 - x(1-x)m_Z^2}{m_{\phi^\pm}^2} \right\} . \tag{27}
\end{aligned}$$

V. NUMERICAL ANALYSIS

As mentioned above, the most stringent constraint on the parameter space is that the 3×3 mass squared matrix in Eq.(5) should produce the lightest eigenvector with a mass $m_{h_0} = 125$ GeV.

In order to make the final results consistent with this condition, we require the self coupling of the Higgs doublet to satisfy

$$\lambda_{HH} = \frac{A}{B}, \quad (28)$$

where

$$\begin{aligned} A &= m_{h_0}^6 - 2[\lambda_{BB}v_B^2 + \lambda_{LL}v_L^2]m_{h_0}^4 + [(4\lambda_{BB}\lambda_{LL} - \lambda_{BL}^2)v_B^2v_L^2 - \lambda_{HB}^2v_B^2v_L^2 \\ &\quad - \lambda_{HL}^2v_B^2v_L^2]m_{h_0}^2 + 2[\lambda_{BB}\lambda_{HL}^2 + \lambda_{LL}\lambda_{HB}^2 - \lambda_{HB}\lambda_{HL}\lambda_{BL}]v_B^2v_L^2, \\ B &= 2v^2[m_{h_0}^4 - 2(\lambda_{BB}v_B^2 + \lambda_{LL}v_L^2)m_{h_0}^2 + (4\lambda_{BB}\lambda_{LL} - \lambda_{BL}^2)v_B^2v_L^2]. \end{aligned} \quad (29)$$

The present experimental lower bounds on the fourth generation charged lepton τ' , up-type and down-type quarks t' and b' at 95 % C.L. are $m_{\tau'} > 100.8$ GeV, $m_{t'} > 420$ GeV and $m_{b'} > 372$ GeV, respectively. The fourth generation quarks t' and b' acquire nonzero masses $m_{t'} = m_{b'} = \frac{Y'_Q}{\sqrt{2}}v_B$ when local $U(1)_B$ symmetry is broken. In addition, the charged leptons of the fourth generation τ' obtains nonzero masses $m_{\tau'} = \frac{Y'_L}{\sqrt{2}}v_L$ when local $U(1)_L$ symmetry is broken.

However, there are too many free parameters in the model considered here. In our numerical analysis, we adopt the assumption on the parameter space

$$\begin{aligned} m_{t'} &= m_{b'} = m_{\tau'} = m_F, \\ \lambda_{BB} &= \lambda_{LL} = 0.5, \quad \lambda_{HL} = \lambda_{BL} = \lambda_{HB} = \lambda_{NP}, \\ \lambda_{\phi H} &= \lambda_{\phi B} = \lambda_{\phi L} = \lambda'_{NP}, \end{aligned} \quad (30)$$

to decrease the number of free parameters in the concerned model. Furthermore, we assume $v \ll v_{B,L}$, $(\lambda_a)_{3 \times 3} = \text{diag}(\lambda_a, \lambda_a, \lambda_a)$, and choose the hierarchical assumption on Yukawa couplings $|(Y_\nu)_{IJ}| \ll |Y'_\nu| \sim \lambda_a \sim \lambda_{b_I}$, ($I, J = 1, 2, 3$) to obtain our final results. Applying the assumptions above, we obtain the majorana mass for the lightest exotic neutrino N_1 to be

$$m_{N_1} \simeq \frac{v^2}{\sqrt{2}v_L} \frac{\lambda_a |Y'_\nu|}{\lambda_b^2}, \quad (31)$$

with $\lambda_b^2 = \lambda_{b_1}^2 + \lambda_{b_2}^2 + \lambda_{b_3}^2$. Of course, we need this mass to be greater than $m_z/2$ to be consistent with the measured Z -boson decay width. The masses of other heavy majorana neutrinos are

$$m_{N_i} \simeq \left(\frac{v_L}{\sqrt{2}}\lambda_a, \frac{v_L}{\sqrt{2}}\lambda_a, \frac{v_L}{2\sqrt{2}}(\Delta - \lambda_a), \frac{v_L}{2\sqrt{2}}(\Delta + \lambda_a) \right), \quad (32)$$

for $i = 2, 3, 4, 5$ and $\Delta = \sqrt{\lambda_a^2 + 4\lambda_b^2}$.

Correspondingly, the 5×5 mixing matrix Z_N is approximated as

$$Z_N \simeq \begin{pmatrix} 1, & -\frac{\lambda_a Y_\nu^* v}{\lambda_b^2 v_L}, & \frac{\lambda_{b_1} Y_\nu^* v}{\lambda_b^2 v_L}, & \frac{\lambda_{b_2} Y_\nu^* v}{\lambda_b^2 v_L}, & \frac{\lambda_{b_3} Y_\nu^* v}{\lambda_b^2 v_L} \\ \frac{\lambda_a Y_\nu^* v}{\lambda_b^2 v_L}, & 0, & 0, & -i\sqrt{\frac{\Delta+\lambda_a}{2\Delta}}, & \sqrt{\frac{\Delta-\lambda_a}{2\Delta}} \\ -\frac{\lambda_{b_1} Y_\nu^* v}{\lambda_b^2 v_L}, & -\frac{\lambda_{b_3}}{\sqrt{\lambda_{b_1}^2 + \lambda_{b_3}^2}}, & -\frac{\lambda_{b_2}}{\sqrt{\lambda_{b_1}^2 + \lambda_{b_2}^2}}, & \frac{i\sqrt{2}\lambda_{b_1}}{\sqrt{\Delta^2 + \lambda_a \Delta}}, & \frac{\sqrt{2}\lambda_{b_1}}{\sqrt{\Delta^2 - \lambda_a \Delta}} \\ -\frac{\lambda_{b_2} Y_\nu^* v}{\lambda_b^2 v_L}, & 0, & 0, & \frac{i\sqrt{2}\lambda_{b_2}}{\sqrt{\Delta^2 + \lambda_a \Delta}}, & \frac{\sqrt{2}\lambda_{b_2}}{\sqrt{\Delta^2 - \lambda_a \Delta}} \\ -\frac{\lambda_{b_3} Y_\nu^* v}{\lambda_b^2 v_L}, & \frac{\lambda_{b_1}}{\sqrt{\lambda_{b_1}^2 + \lambda_{b_3}^2}}, & \frac{\lambda_{b_1}}{\sqrt{\lambda_{b_1}^2 + \lambda_{b_2}^2}}, & \frac{i\sqrt{2}\lambda_{b_3}}{\sqrt{\Delta^2 + \lambda_a \Delta}}, & \frac{\sqrt{2}\lambda_{b_3}}{\sqrt{\Delta^2 - \lambda_a \Delta}} \end{pmatrix}. \quad (33)$$

For the relevant parameters in the SM, we take [13]

$$\begin{aligned} \alpha_s(m_z) &= 0.118, \quad \alpha(m_z) = 1/128, \\ s_w^2(m_z) &= 0.23, \quad m_t = 174.2 \text{ GeV}, \quad m_w = 80.4 \text{ GeV}. \end{aligned} \quad (34)$$

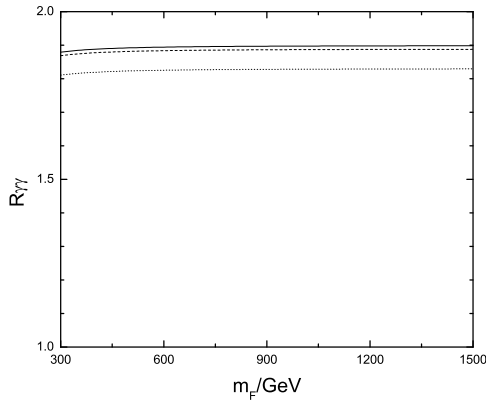


FIG. 1: Variation of $R_{\gamma\gamma}$ with the mass scale of exotic fermions m_F when $m_{\phi^\pm} = 500\text{GeV}$, $\lambda_{NP} = 0.5$, $\lambda'_{NP} = -0.5$. The dotted line represents $v_B = v_L = 500 \text{ GeV}$, the dashed line represents $v_B = v_L = 1000 \text{ GeV}$, and the solid line represents $v_B = v_L = 1500 \text{ GeV}$.

A. Numerical results of $R_{\gamma\gamma}$

Under our assumptions on the parameter space, the theoretical prediction of $R_{\gamma\gamma}$ depends on six parameters in the model: m_F , m_{ϕ^\pm} , λ_{NP} , λ'_{NP} , v_B and v_L . Taking $m_{\phi^\pm} = 500\text{GeV}$, $\lambda_{NP} = 0.5$ and $\lambda'_{NP} = -0.5$, we plot the variation of $R_{\gamma\gamma}$ with the

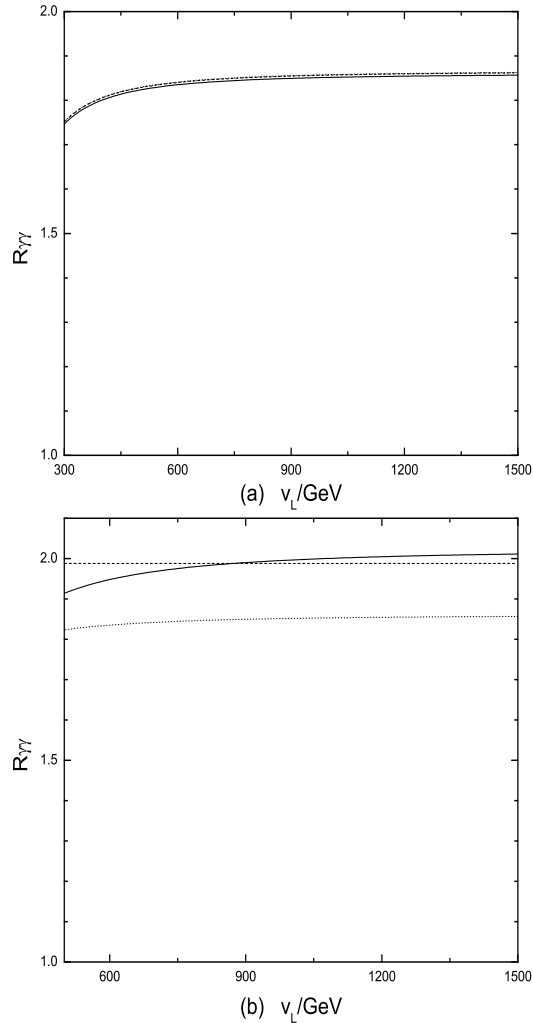


FIG. 2: Variation of $R_{\gamma\gamma}$ with the VEV v_L when $m_{\phi^\pm} = v_B = 500\text{GeV}$, $\lambda'_{NP} = -0.5$. In (a), $\lambda_{NP} = 0.5$, the dotted line corresponds to $m_F = 500\text{GeV}$, the dashed line corresponds to $m_F = 550\text{ GeV}$, and the solid line corresponds to $m_F = 600\text{ GeV}$. In (b), $m_F = 500\text{GeV}$, the dotted line corresponds to $\lambda_{NP} = 0.5$, the dashed line corresponds to $\lambda_{NP} = 0$, and the solid line corresponds to $\lambda_{NP} = -0.5$.

mass scalar of exotic fermions M_F , as shown in Fig.1. The dotted line corresponds to $v_B = v_L = 500$ GeV, the dashed line corresponds to $v_B = v_L = 1000$ GeV, and the solid line corresponds to $v_B = v_L = 1500$ GeV. In general, the ratio $R_{\gamma\gamma}$ depends very weakly on the mass scale m_F , and the value of $R_{\gamma\gamma}$ is about $1.8 \sim 1.9$ when $500 \text{ GeV} \leq v_B = v_L \leq 1500 \text{ GeV}$.

In Fig. 2(a), we plot the variation of $R_{\gamma\gamma}$ with the VEV v_L when $m_{\phi^\pm} = v_B = 500$ GeV, $\lambda'_{NP} = -0.5$ and $\lambda_{NP} = 0.5$. The dotted line corresponds to $m_F = 500$ GeV, the

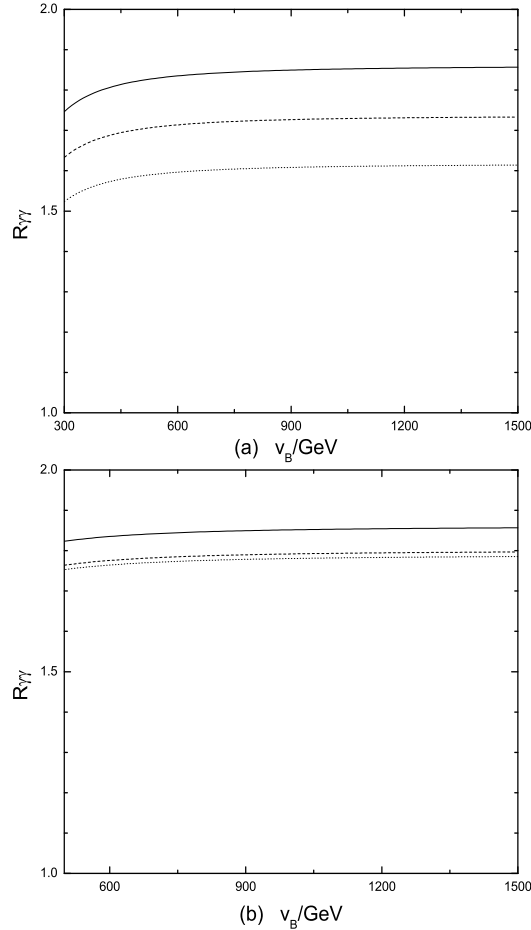


FIG. 3: Variation of $R_{\gamma\gamma}$ with the VEV v_B when $m_F = v_L = 500$ GeV, $\lambda_{NP} = 0.5$ for: (a) $m_{\phi^\pm} = 500$ GeV, where the dotted line corresponds to $\lambda'_{NP} = 0.5$, the dashed line corresponds to $\lambda'_{NP} = 0$, and the solid line corresponds to $\lambda'_{NP} = -0.5$; (b) $\lambda'_{NP} = -0.5$, where the dotted line corresponds to $m_{\phi^\pm} = 1500$ GeV, the dashed line corresponds to $m_{\phi^\pm} = 1000$ GeV, and the solid line corresponds to $m_{\phi^\pm} = 500$ GeV.

dashed line corresponds to $m_F = 550$ GeV, and the solid line corresponds to $m_F = 600$ GeV. The dependence of $R_{\gamma\gamma}$ on v_L is relatively sensitive for $v_L \leq 600$ GeV, and is weak for $v_L > 600$ GeV. Since the dependence of $R_{\gamma\gamma}$ on m_F and v_B is very weak, the three lines almost coincide with each other. In Fig. 2(b), we plot the variation of $R_{\gamma\gamma}$ with the VEV v_L when $m_F = m_{\phi^\pm} = v_B = 500$ GeV, $\lambda'_{NP} = -0.5$. The dotted line corresponds to $\lambda_{NP} = 0.5$, the dashed line corresponds to $\lambda_{NP} = 0$, and the solid line corresponds to $\lambda_{NP} = -0.5$. Generally, there is a weak dependence of the ratio $R_{\gamma\gamma}$ on v_L .

In Fig. 3(a), we show the variation of $R_{\gamma\gamma}$ with the VEV v_B when $m_F = v_L = 500$ GeV, $\lambda_{NP} = 0.5$. The dotted line corresponds to $\lambda'_{NP} = 0.5$, the dashed line corresponds to $\lambda'_{NP} = 0$, and the solid line corresponds to $\lambda'_{NP} = -0.5$. The dependence of $R_{\gamma\gamma}$ on v_B is relatively sensitive for $v_B \leq 600$ GeV, and is weak for $v_B > 600$ GeV. In Fig. 3(b), we show the variation of $R_{\gamma\gamma}$ with v_B when $m_F = v_L = 500$ GeV, $\lambda'_{NP} = -0.5$ and $\lambda_{NP} = 0.5$. The dotted line corresponds to $m_{\phi^\pm} = 1500$ GeV, the dashed line corresponds to $m_{\phi^\pm} = 1000$ GeV, and the solid line corresponds to $m_{\phi^\pm} = 500$ GeV. Generally, there is a very weak dependence of the ratio $R_{\gamma\gamma}$ on v_B .

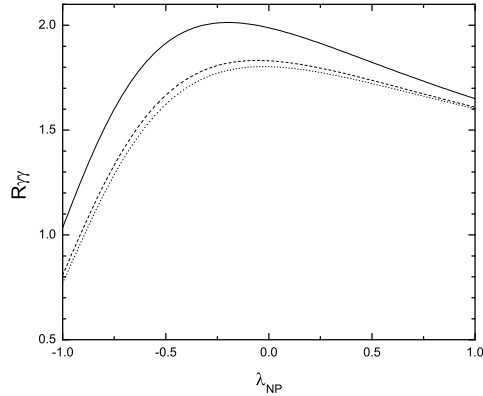


FIG. 4: Variation of $R_{\gamma\gamma}$ with λ_{NP} when $v_B = v_L = 500$ GeV, $\lambda'_{NP} = -0.5$, where the dotted line represents $m_F = 500$ GeV, $m_{\phi^\pm} = 1500$ GeV, the dashed line represents $m_F = 550$ GeV, $m_{\phi^\pm} = 1000$ GeV, and the solid line represents $m_F = m_{\phi^\pm} = 500$ GeV.

Choosing $v_B = v_L = 500$ GeV, $\lambda'_{NP} = -0.5$, Fig.4 presents the variation of the ratio $R_{\gamma\gamma}$ with λ_{NP} . The dotted line represents $m_F = 500$ GeV, $m_{\phi^\pm} = 1500$ GeV, the dashed line represents $m_F = 550$ GeV, $m_{\phi^\pm} = 1000$ GeV, and the solid line represents $m_F = m_{\phi^\pm} = 500$ GeV. As λ_{NP} increases, $R_{\gamma\gamma}$ changes drastically and can easily coincide with the present experimental data, as $-0.5 \leq \lambda_{NP} \leq 1.0$. Choosing $m_F = v_B = v_L = 500$ GeV, and $\lambda_{NP} =$

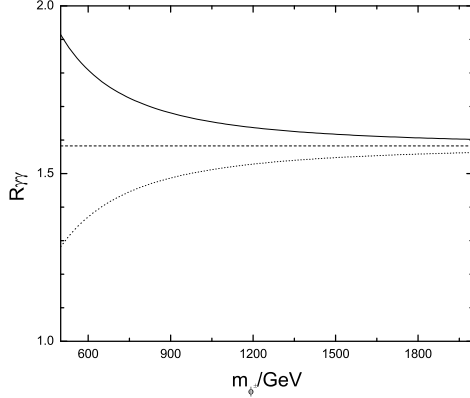


FIG. 5: Variation of $R_{\gamma\gamma}$ with m_{ϕ^\pm} when $m_F = v_B = v_L = 500$ GeV, $\lambda_{NP} = -0.5$, where the dotted line represents $\lambda'_{NP} = 0.5$, the dashed line represents $\lambda'_{NP} = 0$, and the solid line represents $\lambda'_{NP} = -0.5$.

-0.5 , Fig.5 shows the ratio $R_{\gamma\gamma}$ versus m_{ϕ^\pm} . The dotted line represents $\lambda'_{NP} = 0.5$, the dashed line represents $\lambda'_{NP} = 0$, and the solid line represents $\lambda'_{NP} = -0.5$. For $\lambda'_{NP} = 0$, there is a slight dependence of $R_{\gamma\gamma}$ on the mass m_{ϕ^\pm} . When $\lambda'_{NP} = \pm 0.5$, $R_{\gamma\gamma}$ decreases steeply as m_{ϕ^\pm} increases.

In Fig. 6, we plot the variation of the ratio $R_{\gamma\gamma}$ with λ'_{NP} when $m_F = v_B = v_L = 500$ GeV and $\lambda_{NP} = -0.5$. The dotted line represents $m_{\phi^\pm} = 1500$ GeV, the dashed line represents $m_{\phi^\pm} = 1000$ GeV, and the solid line represents $m_{\phi^\pm} = 500$ GeV. The dependence of $R_{\gamma\gamma}$ on λ'_{NP} is strong when $m_{\phi^\pm} = 500$ GeV but weaker for higher values of m_{ϕ^\pm} .

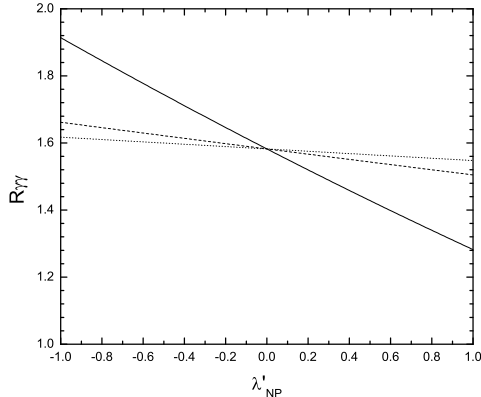


FIG. 6: Variation of $R_{\gamma\gamma}$ with λ'_{NP} when $m_F = v_B = v_L = 500$ GeV, $\lambda_{NP} = -0.5$, where the dotted line represents $m_{\phi^\pm} = 1500$ GeV, the dashed line represents $m_{\phi^\pm} = 1000$ GeV, and the solid line represents $m_{\phi^\pm} = 500$ GeV.

Generally, the ratio $R_{\gamma\gamma}$ depends strongly on the parameters λ_{NP} , λ'_{NP} and m_{ϕ^\pm} , and depends weakly on v_B, v_L and m_F . These numerical results can be reasonably explained from Eq.(18) and Eq.(19), where λ_{NP} affects theoretical predictions of $R_{\gamma\gamma}$ through the 3×3 mixing matrix Z_{CPE} , while λ'_{NP} and m_{ϕ^\pm} affect theoretical predictions of $R_{\gamma\gamma}$ through the last term in Eq.(19).

The important point is that the parameters λ_a, λ_{b_i} ($i = 1, 2, 3$) do not affect the theoretical predictions of $R_{\gamma\gamma}$ since there is no correction to the decay widths of $h_0 \rightarrow \gamma\gamma$ and $h_0 \rightarrow gg$ from the neutrino sector at one-loop level. Similarly, the parameters M_S, μ_1, μ_2 also do not affect theoretical evaluations of $R_{\gamma\gamma}$, as there is no one-loop correction to the decay widths of $h_0 \rightarrow \gamma\gamma$ and $h_0 \rightarrow gg$ from virtual Φ_i^0 ($i = 1, 2, 3, 4$).

B. The constraints on parameter space from oblique corrections

The heavy neutrinos contribute one-loop radiative corrections to the self energies of $ZZ, W^\pm W^\mp$ in this model. This results in the theoretical values of the S, T, U parameters depending on λ_a, λ_{b_i} ($i = 1, 2, 3$) here. Furthermore, the theoretical values of the S, T, U parameters also depend on m_S, μ_1, μ_2 through the virtual ϕ^\pm, Φ_i^0 , ($i = 1, 2, 3, 4$) radiative corrections to the self energies of $ZZ, W^\pm W^\mp$ at one-loop level. So far, fitting S, T, U within 3σ deviation indicates

$$\begin{aligned} -0.26 &\leq \Delta S \leq 0.34, \\ -0.28 &\leq \Delta T \leq 0.38, \\ -0.25 &\leq \Delta U \leq 0.41. \end{aligned} \tag{35}$$

In order to obtain theoretical values of S, T, U which satisfy present experimental data, we adopt the additional assumptions here:

$$\begin{aligned} m_{N_1} &\simeq \frac{v^2}{\sqrt{2}v_L} \frac{\lambda_a |Y'_\nu|}{\lambda_b^2} = m_F, \\ \lambda_{b_1} &= \lambda_{b_2} = \lambda_{b_3} = \frac{1}{\sqrt{3}} \lambda_b, \\ v_B &= v_L = m_S = m_F = 500 \text{ GeV}, \\ |\mu_1| &= 20 \text{ GeV}, |\mu_2| = 200 \text{ GeV}, \\ \lambda_a &= \lambda_b = 0.6, \lambda_{BB} = \lambda_{LL} = 0.5, \lambda_{NP} = \lambda'_{NP} = 0.01. \end{aligned} \tag{36}$$

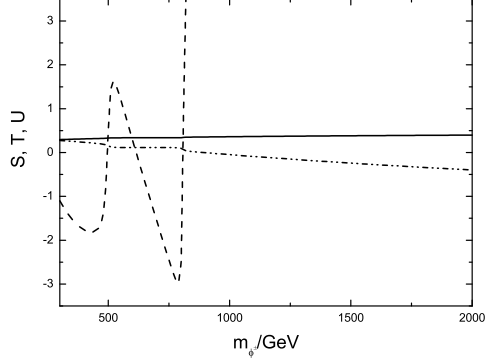


FIG. 7: Adopting the assumptions mentioned in the text and assuming $\theta_1 = \arg(\mu_1) = \pi$, $\theta_2 = \arg(\mu_2) = \pi/4$, we present the theoretical values for a) ΔS (solid line), b) ΔU (dash-dot-dot line), and c) ΔT (dashed line) versus the mass m_{ϕ^\pm} .

Choosing $\theta_1 = \arg(\mu_1) = \pi$, $\theta_2 = \arg(\mu_2) = \pi/4$, we depict the theoretical values of ΔS , ΔU , ΔT versus the mass of charged scalar ϕ^\pm in Fig.(7), in which the solid line represents ΔS , the dash-dot-dot line represents ΔU , and the dashed line represents ΔT . For our choices of the relevant parameters, the theoretical value of ΔT is very sensitive to the mass m_{ϕ^\pm} , while the theoretical values of ΔS and ΔU have a weak dependence on the mass m_{ϕ^\pm} . When the mass of the charged scalar lies in the range $400 \leq m_{\phi^\pm}/\text{GeV} \leq 700$, the theoretical predictions of ΔS , ΔT , ΔU simultaneously satisfy the inequalities in Eq.(35). The CP phases θ_1 , θ_2 also affect the numerical results of ΔS , ΔU , ΔT through the 4×4

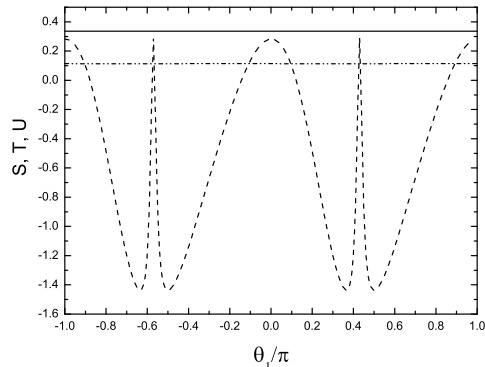


FIG. 8: Adopting the assumptions mentioned in the text and assuming $m_{\phi^\pm} = 600$ GeV, $\theta_2 = \arg(\mu_2) = \pi/4$, we present the theoretical values of a) ΔS (solid line), b) ΔU (dash-dot-dot line), and c) ΔT (dashed line) versus the CP phase $\theta_1 = \arg(\mu_1)$.

mixing matrix Z_{CPM} . Taking $m_{\phi\pm} = 600$ GeV and $\theta_2 = \pi/4$, we present the theoretical evaluations on ΔS , ΔU , ΔT versus the CP phase θ_1 in Fig.(8). With our assumptions on the parameter space, the theoretical value of ΔT varies strongly with the CP phase θ_1 , while the theoretical values of ΔS and ΔU vary weakly with the CP phase θ_1 . In the neighbourhoods of $\theta_1 = 0, \pm\pi/2, \pm\pi$, the theoretical predictions on ΔS , ΔT , ΔU simultaneously lie within the ranges presented in Eq.(35).

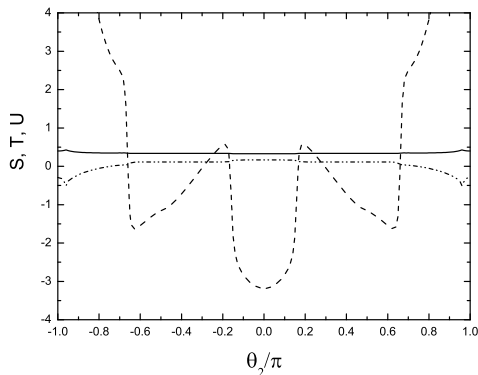


FIG. 9: Adopting the mentioned assumptions in text and assuming $m_{\phi\pm} = 600$ GeV, $\theta_1 = \arg(\mu_1) = \pi$, we present the theoretical values of a) ΔS (solid line), b) ΔU (dash-dot-dot line), and c) ΔT (dashed line) versus the CP phase $\theta_2 = \arg(\mu_2)$.

In Fig. 9, we present the theoretical values of ΔS , ΔT , ΔU varying with the CP phase θ_2 when $m_{\phi\pm} = 600$ GeV and $\theta_1 = \pi$. As the CP phase θ_2 varies, the theoretical value of ΔT changes drastically, while the theoretical values of ΔS and ΔU change slowly. In the neighbourhoods around $\theta_2 = \pm\pi/4, \pm3\pi/4$, the theoretical predictions of ΔS , ΔT , ΔU coincide with the present global EWPD fit within 3σ deviations.

VI. SUMMARY

For an extension of the SM with local gauged baryon and lepton numbers, we have discussed the constraints from the oblique parameters S , T , U when the lightest Higgs has a mass around 125 GeV. Considering those constraints, we find that there is parameter space to account for the excess in Higgs production and decay in the diphoton channel observed in the ATLAS and CMS experiments. Of course, our numerical results strongly depend on the assumptions made on the model considered here. In other words, our theoretical prediction cannot be precise because of the theoretical uncertainties. The purpose of our calculation

is to show that this extension of the SM may be still right after the constraints from LHC data on the Higgs and oblique parameters have been taken into account.

Appendix A: Higgs masses and relevant couplings

After diagonalizing the mass matrix Eq.(5), we obtain

$$\begin{aligned} m_{h_0}^2 &= \text{Min}(m_1^2, m_2^2, m_3^2) \\ m_{H_3^0}^2 &= \text{Max}(m_1^2, m_2^2, m_3^2) \end{aligned} \quad (\text{A1})$$

with

$$\begin{aligned} m_1^2 &= -\frac{a}{3} + \frac{2}{3}p \cos \phi, \\ m_2^2 &= -\frac{a}{3} - \frac{1}{3}p(\cos \phi - \sqrt{3} \sin \phi), \\ m_3^2 &= -\frac{a}{3} - \frac{1}{3}p(\cos \phi + \sqrt{3} \sin \phi). \end{aligned} \quad (\text{A2})$$

To formulate the expressions in a concise form, we define the notations

$$p = \sqrt{a^2 - 3b}, \quad \phi = \frac{1}{3} \arccos\left(-\frac{1}{p^3}\left(a^3 - \frac{9}{2}ab + \frac{27}{2}c\right)\right) \quad (\text{A3})$$

where

$$\begin{aligned} a &= -2(\lambda_{HH}v^2 + \lambda_{BB}v_B^2 + \lambda_{LL}v_L^2), \\ b &= 4(\lambda_{HH}\lambda_{BB}v^2v_B^2 + \lambda_{HH}\lambda_{LL}v^2v_L^2 + \lambda_{BB}\lambda_{LL}v_B^2v_L^2) \\ &\quad - \lambda_{HB}^2v^2v_B^2 - \lambda_{HL}^2v^2v_L^2 - \lambda_{BL}^2v_B^2v_L^2, \\ c &= 2(\lambda_{HH}\lambda_{BL}^2 + \lambda_{BB}\lambda_{HL}^2 + \lambda_{LL}\lambda_{HB}^2 - 4\lambda_{HH}\lambda_{BB}\lambda_{LL} \\ &\quad - \lambda_{HB}\lambda_{HL}\lambda_{BL})v^2v_B^2v_L^2. \end{aligned} \quad (\text{A4})$$

The normalized eigenvectors of the mass squared matrix in Eq.(5) are given by

$$\begin{aligned} \begin{pmatrix} (Z_{CPE})_{11} \\ (Z_{CPE})_{21} \\ (Z_{CPE})_{31} \end{pmatrix} &= \frac{1}{\sqrt{|X_1|^2 + |Y_1|^2 + |Z_1|^2}} \begin{pmatrix} X_1 \\ Y_1 \\ Z_1 \end{pmatrix}, \\ \begin{pmatrix} (Z_{CPE})_{12} \\ (Z_{CPE})_{22} \\ (Z_{CPE})_{32} \end{pmatrix} &= \frac{1}{\sqrt{|X_2|^2 + |Y_2|^2 + |Z_2|^2}} \begin{pmatrix} X_2 \\ Y_2 \\ Z_2 \end{pmatrix}, \end{aligned}$$

$$\begin{pmatrix} (Z_{CPE})_{13} \\ (Z_{CPE})_{23} \\ (Z_{CPE})_{33} \end{pmatrix} = \frac{1}{\sqrt{|X_3|^2 + |Y_3|^2 + |Z_3|^2}} \begin{pmatrix} X_3 \\ Y_3 \\ Z_3 \end{pmatrix}, \quad (\text{A5})$$

with

$$\begin{aligned} X_1 &= (2\lambda_{BB}v_B^2 - m_1^2)(2\lambda_{LL}v_L^2 - m_1^2) - \lambda_{BL}^2 v_B^2 v_L^2, \\ Y_1 &= \lambda_{HL}\lambda_{BL}vv_Bv_L^2 - \lambda_{HB}vv_B(2\lambda_{LL}v_L^2 - m_1^2), \\ Z_1 &= \lambda_{HB}\lambda_{BL}vv_B^2v_L - \lambda_{HL}vv_L(2\lambda_{BB}v_B^2 - m_1^2), \\ X_2 &= \lambda_{HL}\lambda_{BL}vv_Bv_L^2 - \lambda_{HB}vv_B(2\lambda_{LL}v_L^2 - m_2^2), \\ Y_2 &= (2\lambda_{HH}v^2 - m_2^2)(2\lambda_{LL}v_L^2 - m_2^2) - \lambda_{HL}^2 v^2 v_L^2, \\ Z_2 &= \lambda_{HB}\lambda_{HL}v^2v_Bv_L - \lambda_{BL}v_Bv_L(2\lambda_{HH}v^2 - m_2^2), \\ X_3 &= \lambda_{HB}\lambda_{BL}vv_B^2v_L - \lambda_{HL}vv_L(2\lambda_{BB}v_B^2 - m_3^2), \\ Y_3 &= \lambda_{HB}\lambda_{HL}v^2v_Bv_L - \lambda_{BL}v_Bv_L(2\lambda_{HH}v^2 - m_3^2), \\ Z_3 &= (2\lambda_{HH}v^2 - m_3^2)(2\lambda_{BB}v_B^2 - m_3^2) - \lambda_{HB}^2 v^2 v_B^2. \end{aligned} \quad (\text{A6})$$

Appendix B: The loop functions

The loop functions in Eq.(18) and Eq.(19) are given as

$$\begin{aligned} A_1(x) &= -[2x^2 + 3x + 3(2x - 1)g(x)]/x^2, \\ A_{1/2}(x) &= 2[x + (x - 1)g(x)]/x^2, \\ A_0(x) &= -(x - g(x))/x^2, \end{aligned} \quad (\text{B1})$$

with

$$g(x) = \begin{cases} \arcsin^2 \sqrt{x}, & x \leq 1 \\ -\frac{1}{4} \left[\ln \frac{1 + \sqrt{1-1/x}}{1 - \sqrt{1-1/x}} - i\pi \right]^2, & x > 1 \end{cases} \quad (\text{B2})$$

-
- [1] M. E. Peskin and T. Takeuchi, Phys. Rev. Lett. 1999, **65**: 964; Phys. Rev. D, 1992, **46**: 381;
W. J. Marciano and J. L. Rosner, Phys. Rev. Lett. 1999, **65**: 2963.

- [2] B. Holdom and J. Terning, Phys. Lett. B, 1990, **247**: 88; M. Golden and L. Randall, Nucl. Phys. B, 1991, **361**: 3; G. Altarelli and R. Barbieri, Phys. Lett. B, 1990, **253**: 161; G. Altarelli, R. Barbieri and S. Jadach, Nucl. Phys. B, 1992, **369**: 3.
- [3] P. Minkoski, Phys. Lett. B, 1977, **67**: 421; T. Yanagida, Proceedings of the Workshop on the Unified Theory and the Baryon Number in the Universe, KEK, Tsukuba, 1979, p. 95; M. Gell-Mann, P. Ramond, and R. Slansky, Supergravity, North-Holland, Amsterdam, 1979, p315; S. L. Glashow, Quarks and Leptons, Cargése, Plenum, New York, 1980, p707; R. N. Mohapatra and G. Senjanovic, Phys. Rev. Lett. 1980, **44**: 912.
- [4] P. F. Perez and M. B. Wise, Phys. Rev. D, 2010, **82**: 011901; *ibid.* 2011, **84**: 055015; T. R. Dulaney, P. F. Perez and M. B. Wise, Phys. Rev. D, 2011, **83**: 023520; C.-H. Chang, T.-F. Feng, Eur. Phys. J. C, 2000, **12**: 137.
- [5] P. F. Perez, Phys. Lett. B, 2012, **711**: 353; J. M. Arnold, P. F. Perez, B. Fornal, and S. Spinner, Phys. Rev. D, 2012, **85**: 115024.
- [6] C. Anastasiou and K. Melnikov, Nucl. Phys. B, 2002, **646**: 220.
- [7] J. R. Ellis, M. K. Gaillard and D. V. Nanopoulos, Nucl. Phys. B, 1976, **106**: 292; M. A. Shifman, A. I. Vainshtein, M. B. Voloshin and V. I. Zakharov, Sov. J. Nucl. Phys. 1979, **30**: 711; A. Djouadi, Phys. Rept. 2008, **459**: 1; J. F. Gunion, H. E. Haber, G. L. Kane and S. Dawson, *The Higgs Hunter's Guide*, Addison-Wesley, Reading (USA), 1990; M. Carena, I. Low and C. E. M. Wagner, arXiv: hep-ph/ 1206.1082.
- [8] CMS Collaboration, CMS-PAS-HIG-12-016.
- [9] ATLAS Collaboration, ATLAS-CONF-2012-092.
- [10] A. Arbey, M. Battaglia, A. Djouadi and F. Mahmoudi, arXiv: hep-ph/ 1207.1348.
- [11] H.-J. He, N. Polonsky, S.-F Su, Phys. Rev. D, 2001, **64**: 053004.
- [12] M. Baak, M. Goebel, J. Haller, A. Hoecker, D. Ludwig, K. Moenig, M. Schott, J. Stelzer, Eur. Phys. J. C, 2012, **72**: 2003.
- [13] J. Beringer *et al.*(Particle Data Group), Phys. Rev. D, 2012, **86**: 010001.